

## Supporting Information

### Functionalizing porous zirconium terephthalate UiO-66(Zr) for natural gas upgrading: A computational exploration

Qingyuan Yang,<sup>a,b</sup> Andrew D. Wiersum,<sup>c</sup> Philip L. Llewellyn,<sup>c</sup> Vincent Guillerm,<sup>d</sup> Christian Serre,<sup>d</sup> Guillaume Maurin<sup>\*a</sup>

<sup>a</sup> Institut Charles Gerhardt Montpellier, UMR CNRS 5253, UM2, ENSCM, Place E. Bataillon, 34095 Montpellier cedex 05 France

<sup>b</sup> Department of chemical Engineering, Beijing University of Chemical Technology, Beijing 100029, China

<sup>c</sup> Laboratoire Chimie Provence, Universités Aix-Marseille I, II et III - CNRS, UMR 6264, Centre de Saint Jérôme, 13397 Marseille, France

<sup>d</sup> Institut Lavoisier, UMR CNRS 8180-Université de Versailles St Quentin en Yvelines, 45 avenue des Etats-Unis, 78035 Versailles, France

\*To whom correspondence should be addressed. [guillaume.maurin@univ-montp2.fr](mailto:guillaume.maurin@univ-montp2.fr)

## 1. Adsorption Experiments for the Single Gases

The adsorption experiments for the single gases CO<sub>2</sub> and CH<sub>4</sub> have been performed on the non-modified UiO-66(Zr) and the amino-functionalized samples. These two materials were prepared according to the procedure described elsewhere.<sup>1</sup> Prior to adsorption experiments, the samples were placed under a secondary vacuum and heated to various temperatures for 16 hours (up to 250 °C). The final sample was then rehydroxylated and further outgassed at room temperature. The adsorption experiments for CO<sub>2</sub> and CH<sub>4</sub> gases were carried out at 303 K up to a maximum pressure of 50 bar using a laboratory made gas dosing system connected to a commercial gravimetric adsorption device (Rubotherm Präzisionsmeßtechnik GmbH).<sup>2</sup> A step by step gas introduction mode was used. Equilibrium was assumed when the variation of weight remains below 0.03% for 20 minutes. A typical adsorption experiment takes *ca.* 24 hours using around 1g of sample.

The microcalorimetry experiments were performed by means of a manometric dosing apparatus linked to the sample cell housed in a Tian-Calvet type microcalorimeter.<sup>3</sup> Around 0.3 g of sample was used for these experiments. Each experiment was repeated at least twice to ensure repeatability. The error on these experiments can be considered as ± 0.5 kJ/mol.

## 2. Crystalline Structures of UiO-66(Zr) and its modified materials studied in this Work

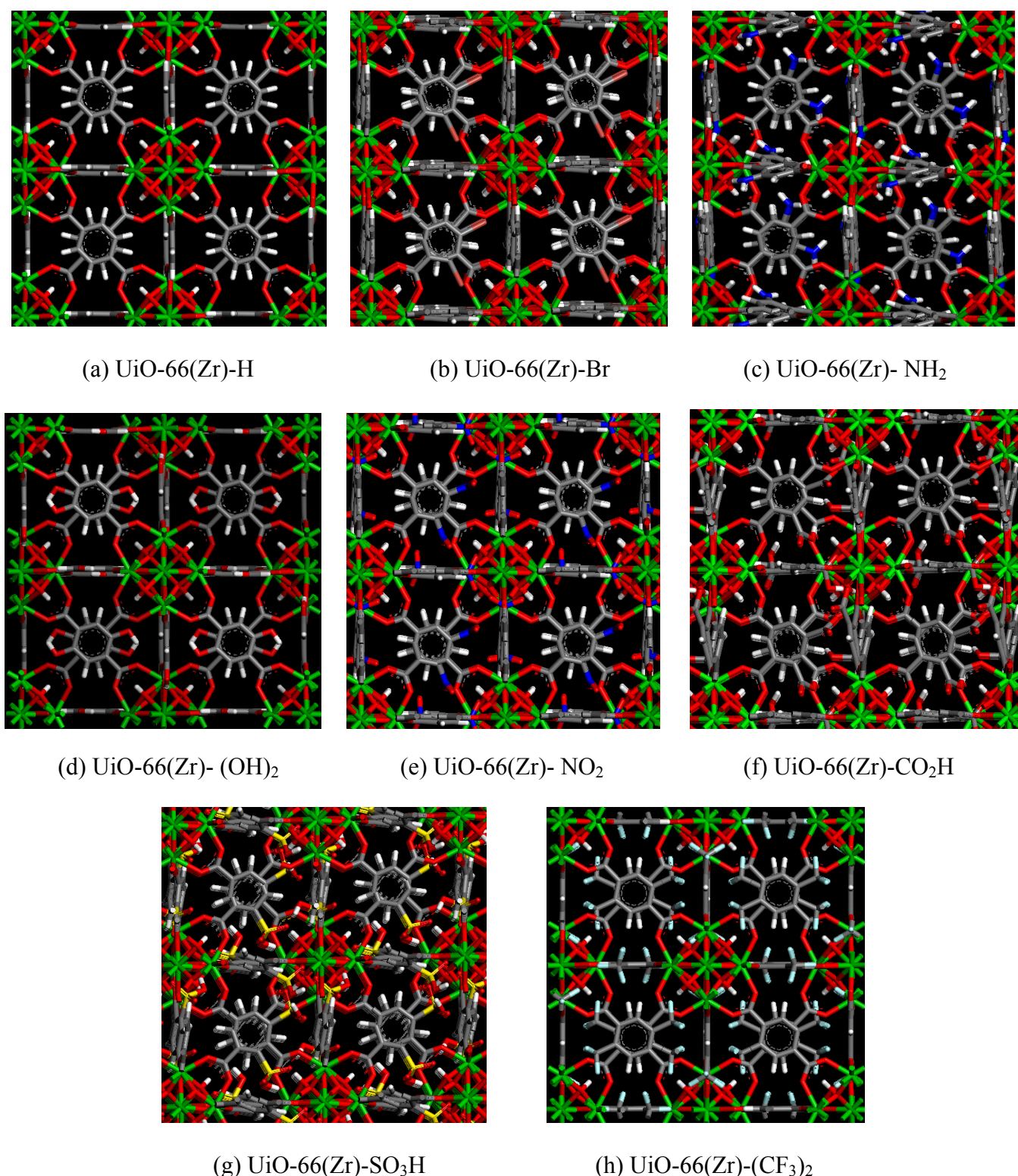


**Fig. S1.** Crystal structures of the UiO-66(Zr) series determined by density functional theory (DFT) geometry optimization based on the experimental unit cell parameters extracted from X-ray diffraction measurements<sup>1</sup>.

**Table S1.** Structural features of the optimized UiO-66(Zr) series obtained by simulations

Materials	Space group <sup>a</sup>	Lattice sizes (Å) <sup>a</sup>	$\rho_{\text{crys}}$ (g/cm <sup>3</sup> ) <sup>c</sup>	$V_{\text{pore}}$ (cm <sup>3</sup> /g) <sup>d</sup>	$S_{\text{acc}}$ (m <sup>2</sup> /g) <sup>d</sup>
UiO-66(Zr)	Fm3m	20.7430	1.238	0.45	1018
UiO-66(Zr)-Br	Pm3m	20.7353	1.592	0.30	535
UiO-66(Zr)-NH <sub>2</sub>	Pm3m	20.7972	1.295	0.40	848
UiO-66(Zr)-(OH) <sub>2</sub>	Fm3m	20.7982	1.370	0.36	737
UiO-66(Zr)-NO <sub>2</sub>	Fm3m	20.8039	1.427	0.32	593
UiO-66(Zr)-CO <sub>2</sub> H <sup>b</sup>	Fm3m	20.8039	1.422	0.31	551
UiO-66(Zr)-SO <sub>3</sub> H	Im3m	20.7487	1.595	0.25	361
UiO-66(Zr)-(CF <sub>3</sub> ) <sub>2</sub>	Fm3m	20.8280	1.823	0.22	334

<sup>a</sup> Obtained from XRD data

<sup>b</sup> Since the experimental unit cell parameter for the material UiO-66(Zr)-CO<sub>2</sub>H is currently not available, we arbitrarily selected those of the UiO-66(Zr)-NO<sub>2</sub> solid. This treatment is reasonable as the lattice parameters only slightly change from one modified form to another as shown in this Table.

<sup>c</sup> These values are the skeleton densities of these crystal structures that were used to calculate the working capacities.

<sup>d</sup> Theoretical calculations.

Based on the parent structure of UiO-66(Zr), the starting configuration for each modified form structure was built by (i) substituting the H atoms on the phenyl rings with the corresponding functional groups, (ii) imposing the unit cell parameters determined from the XRPD refinement (see Tables S1). Further, for each modified form, several initial models were generated by grafting the functional groups onto all the possible positions on the terephthalate linkers. These models were converted into P1 symmetry and then optimized by maintaining the cell parameters fixed. These optimizations were conducted using the Forcite module implemented in Materials Studio software, based on the Universal force field (UFF)<sup>4</sup> and the charges calculated from the Electronegativity Equalization method. For each modified form, the locations for the functional groups were identified by selecting those in the optimized structure with the lowest energy. Finally, density functional theory (DFT) geometry optimization procedure was further employed to refine these selected models, using the Dmol<sup>3</sup> module implemented in

the Materials Studio software. The PW91 GGA functional combined with the double numerical basis set containing polarization function (DNP) were employed in these calculations.

The pore volumes ( $V_{\text{pore}}$ ) of the adsorbents presented in Table S1 were obtained according to the thermodynamic method proposed by Myers and Monson.<sup>5</sup> For the UiO-66(Zr) series considered in this work, the Universal force field (UFF)<sup>4</sup> force field was used to describe the Lennard-Jones (LJ) interactions of the framework atoms while the LJ parameters for Helium ( $\varepsilon/k_B = 10.9 \text{ K}$ ,  $\sigma = 2.640 \text{ \AA}$ ) were taken from the work of Talu and Myers.<sup>6</sup> The accessible surface area ( $S_{\text{acc}}$ ) is purely based on the geometric topology of the adsorbent and calculated from a simple Monte Carlo integration technique where the center of mass of the probe molecule with hard sphere is “rolled” over the framework surface.<sup>7</sup> In this method, a nitrogen-sized (3.6 Å) probe molecule is randomly inserted around each framework atom of the adsorbent and the fraction of the probe molecules without overlapping with the other framework atoms is then used to calculate the accessible surface area. The LJ size parameters of the framework atoms were the same as those used for the calculations of the pore volume.

Since the experimental surface area and pore volume of the samples for the nonmodified UiO-66(Zr) (1144 m<sup>2</sup>/g and 0.47 cm<sup>3</sup>/g) and -NH<sub>2</sub> functionalized form (998 m<sup>2</sup>/g and 0.40 cm<sup>3</sup>/g) are very close to the theoretical values given in the Table S1, the adsorption experiments were then carried out on these two samples as the above mentioned. The so-obtained experimental data were then used to validate the models/methods adopted in this work.

### 3. Density Functional Theory (DFT) Calculations

Due to the large quadruple moment of CO<sub>2</sub> molecule, many studies have demonstrated that it is very important to take the CO<sub>2</sub>-MOF electrostatic interactions into account, especially for the functionalized MOF materials with polar groups.<sup>8</sup> In this work, density functional theory calculations were performed on the clusters cleaved from the optimized unit cell of each modified UiO-66(Zr) structure that was reported in our previous work.<sup>1a</sup> These clusters include building units (e.g. metal-oxide corner and linker) representative of their respective unit cells. All the terminations were saturated by methyl groups with

standard sp<sub>3</sub> geometry. As in our previous work,<sup>8b</sup> the electrostatic potential (ESP) charges obtained with ChelpG method were used as the atomic partial charges, which has been recognized as the most popular and reliable electrostatic charge calculation method.<sup>9</sup> To that purpose, the density functional theory calculations were carried out by means of the GAUSSIAN 03 program<sup>10</sup> using the Perdew-Burke-Ernzerhof (PBE) exchange and correlation functional. For all these calculations, the basis set LANL2DZ<sup>11</sup> was used for atom Zr, while 6-31+G\* was employed for the rest of the atoms which includes one diffuse and one polarization function on atoms heavier than He. In these calculations, the atomic van der Waals (vdW) radii for the framework nonmetal elements used to fit the ESP charges were taken from the work of Bondi et al.<sup>12</sup> As the metal atom Zr was not treated by Bondi, the vdW radius of it was assigned to be 0.75 Å larger than its covalent radius according to the Pauling's approximation used in the Bondi's article. The covalent radius of this element was adopted from the work of Cordero et al.<sup>13</sup> Similar methods have been employed previously to estimate the ESP charges and binding energies in numbers of MOFs.<sup>8a,b,14</sup> The cleaved clusters with the location of atomic types and resulting charges are shown in Figures S2-S8 and listed in Tables S2-S5 respectively.

### 3.1 Model cluster and atomic partial charges of UiO-66(Zr)

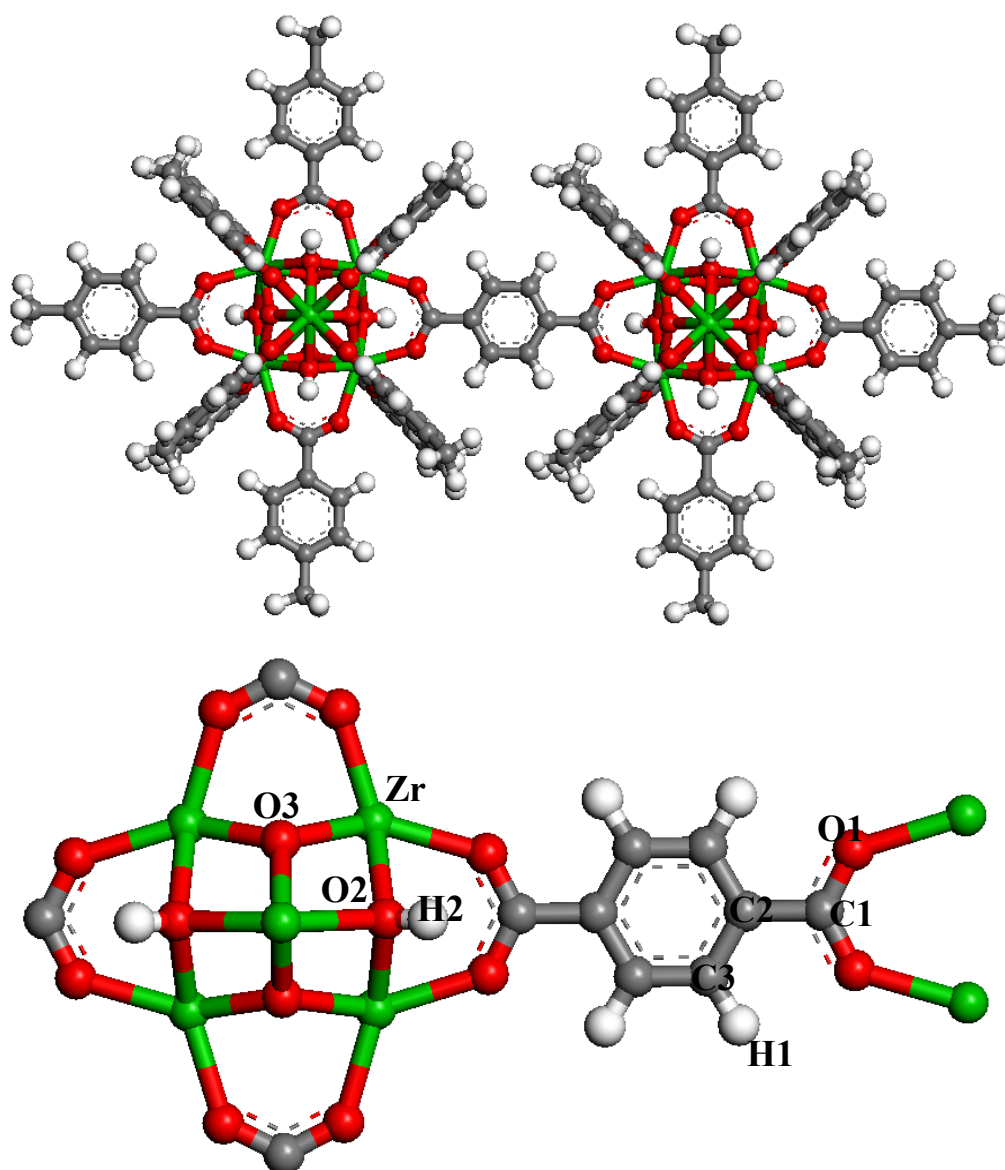


**Fig. S2.** Cluster used for calculating the partial charges for each atom of the UiO-66(Zr) form. The terminations of the cluster were saturated with methyl groups to minimize the boundary effects.

**Table S2.** Atomic partial charges for the UiO-66(Zr) structure derived on DFT/PBE Level.

Atomic types	Zr	O1	O2	O3	C1	C2	C3	H1
Charge (e)	2.008	-0.582	-1.179	-0.741	0.625	-0.002	-0.121	0.127

### 3.2 Model cluster and atomic partial charges of UiO-66(Zr)-Br

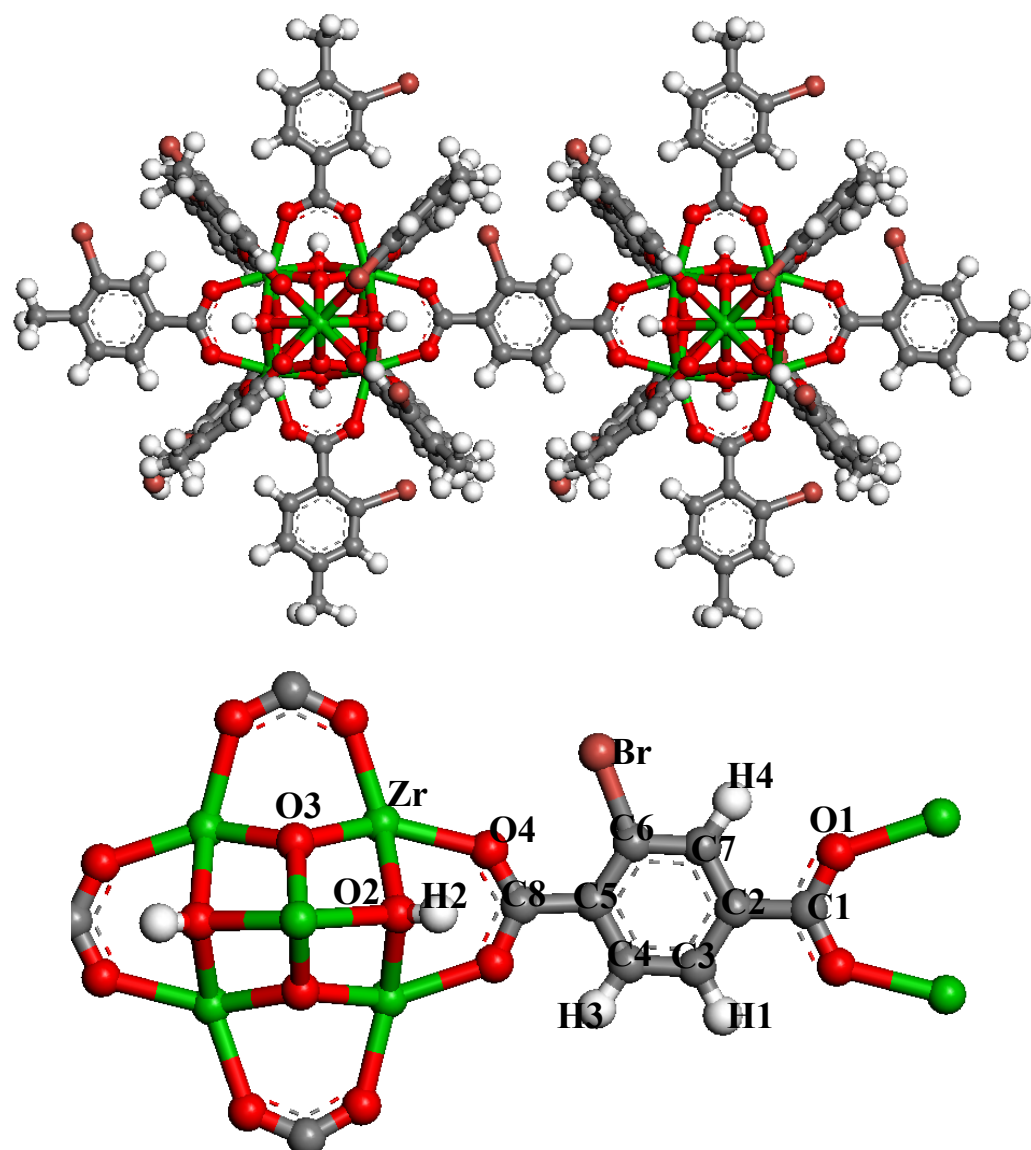


**Fig. S3.** Cluster used for calculating partial charges on UiO-66(Zr)-Br atoms. The terminations of the cluster were saturated with methyl groups to minimize the boundary effects.

**Table S3. Atomic partial charges for the UiO-66(Zr)-Br structure derived on DFT/PBE Level.**

Atomic types	Zr	O1	O2	O3	O4	C1	C2	C3	C4
Charge (e)	2.152	-0.560	-1.051	-0.986	-0.543	0.612	-0.041	-0.088	-0.205
Atomic types	C5	C6	C7	C8	H1	H2	H3	H4	Br
Charge (e)	0.086	-0.038	-0.058	0.572	0.124	0.441	0.151	0.080	-0.060

### 3.3 Model cluster and atomic partial charges of UiO-66(Zr)-NH<sub>2</sub>

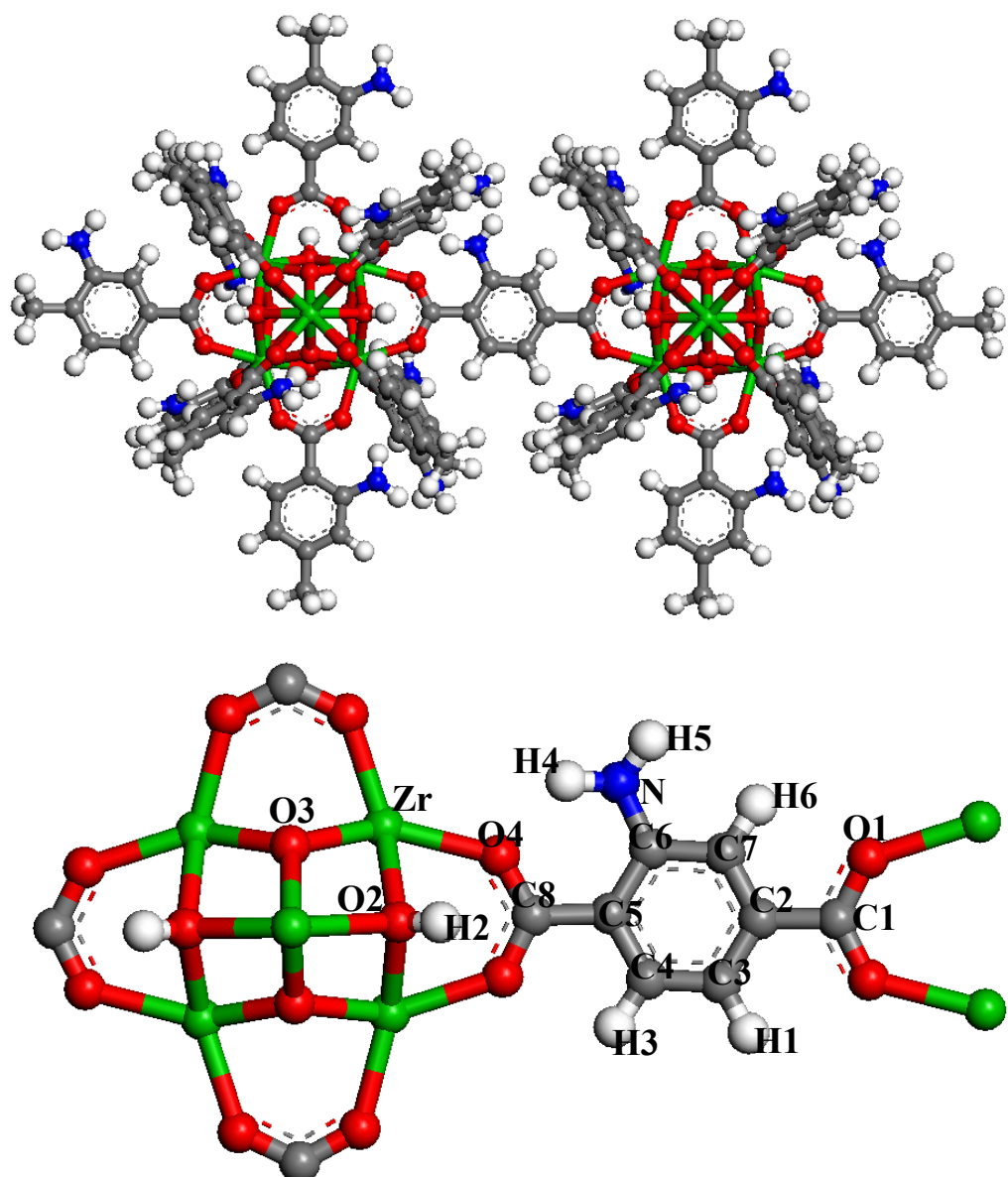


**Fig. S4.** Cluster used for calculating partial charges on UiO-66(Zr)-NH<sub>2</sub> atoms. The terminations of the cluster were saturated with methyl groups to minimize the boundary effects.

**Table S4.** Atomic partial charges for the UiO-66(Zr)-NH<sub>2</sub> structure derived on DFT/PBE Level.

Atomic types	Zr	O1	O2	O3	O4	C1	C2	C3	C4	C5
Charge (e)	2.124	-0.609	-1.037	-0.969	0.617	0.708	-0.007	-0.206	-0.078	-0.256
Atomic types	C6	C7	C8	H1	H2	H3	H4	H5	H6	N
Charge (e)	0.461	-0.320	0.723	0.133	0.434	0.125	0.395	0.368	0.170	-0.848

### 3.4 Model cluster and atomic partial charges of UiO-66(Zr)-(OH)<sub>2</sub>

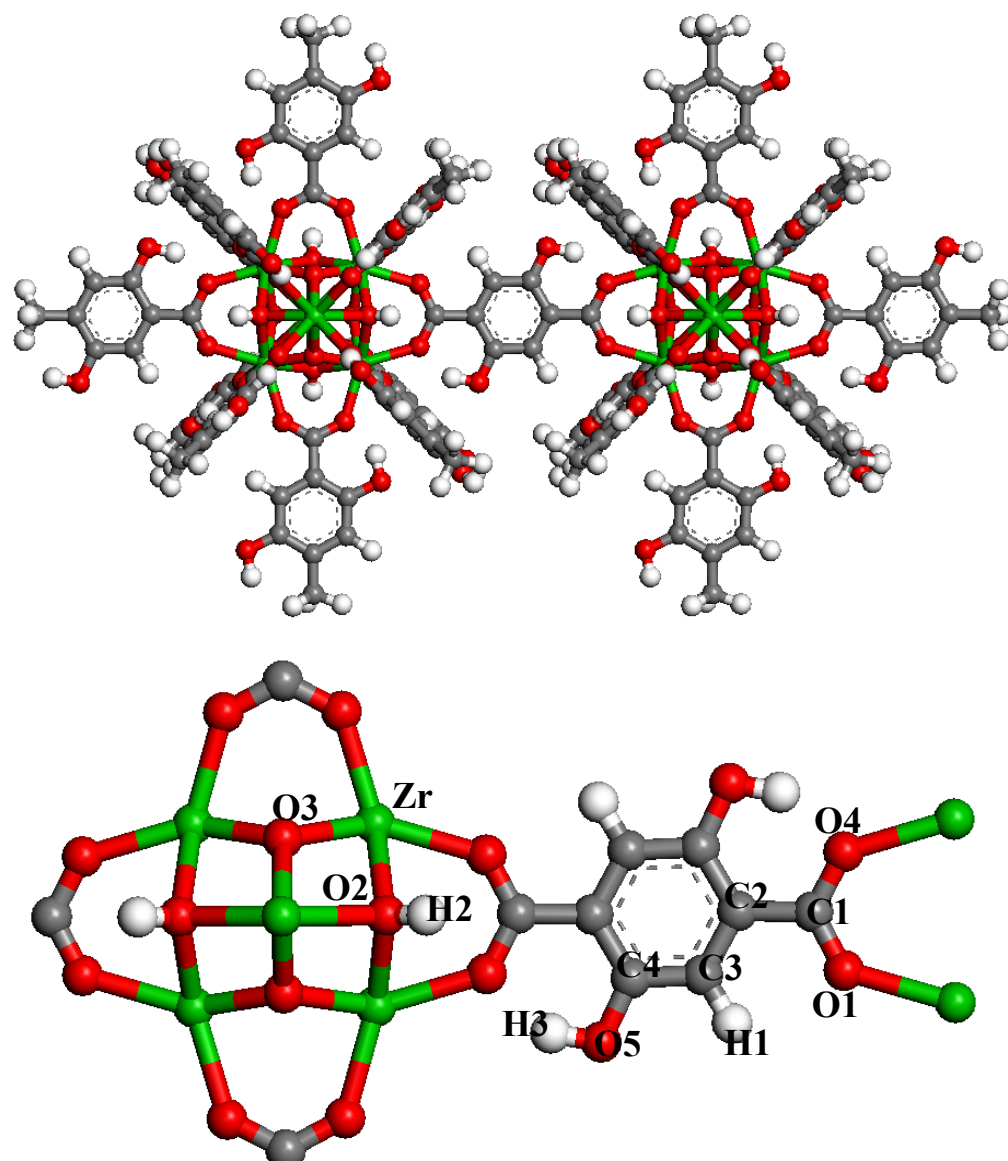
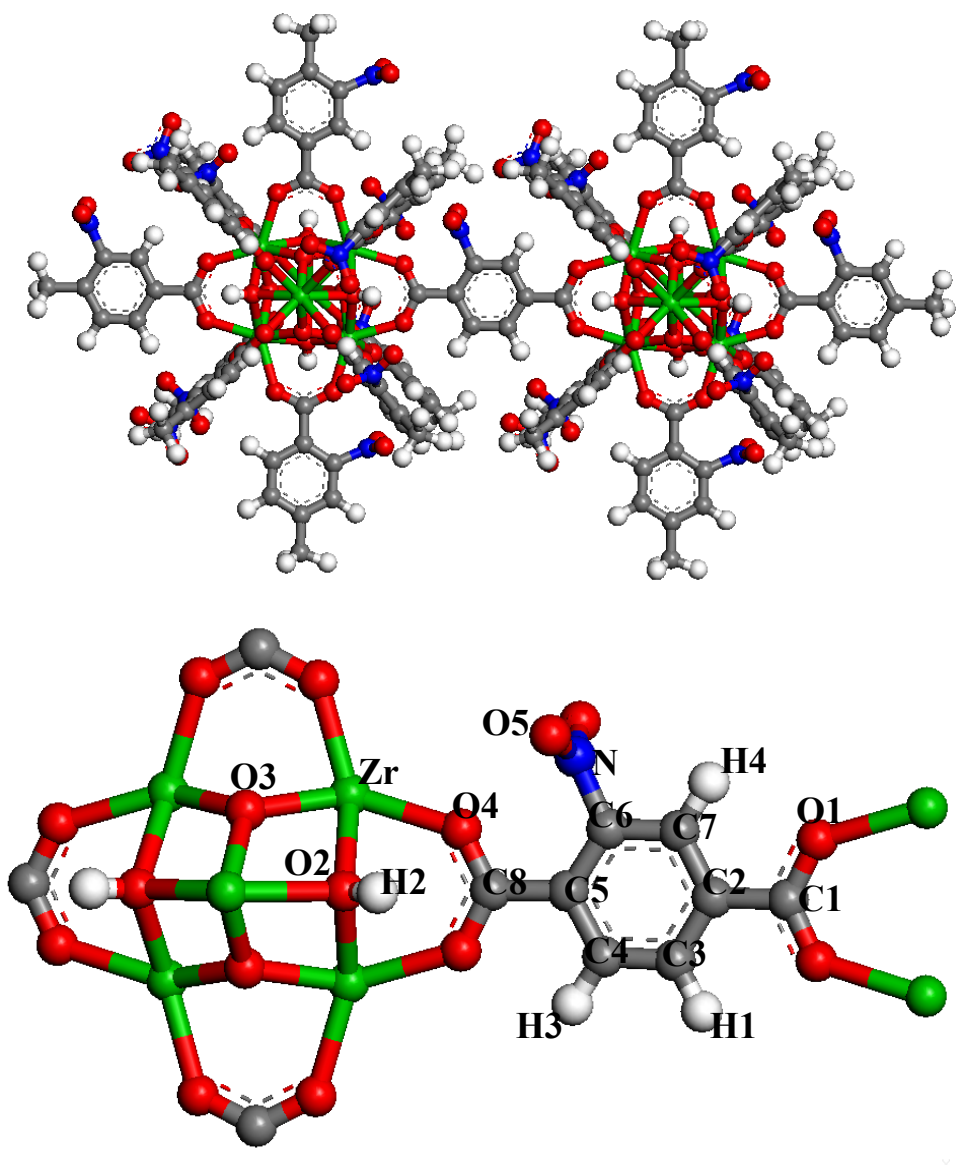


**Fig. S5.** Cluster used for calculating partial charges on UiO-66(Zr)-(OH)<sub>2</sub> atoms. The terminations of the cluster were saturated with methyl groups to minimize the boundary effects.

**Table S5.** Atomic partial charges for the UiO-66(Zr)-(OH)<sub>2</sub> structure derived on DFT/PBE Level.

Atomic types	Zr	O1	O2	O3	O4	O5	C1	C2
Charge (e)	2.396	-0.609	-1.390	-1.011	-0.679	-0.604	0.802	-0.324
Atomic types	C3	C4	H1	H2	H3			
Charge (e)	-0.195	0.404	0.180	0.532	0.450			

### 3.5 Model cluster and atomic partial charges of UiO-66(Zr)-NO<sub>2</sub>



### 3.6 Model cluster and atomic partial charges of UiO-66(Zr)-CO<sub>2</sub>H

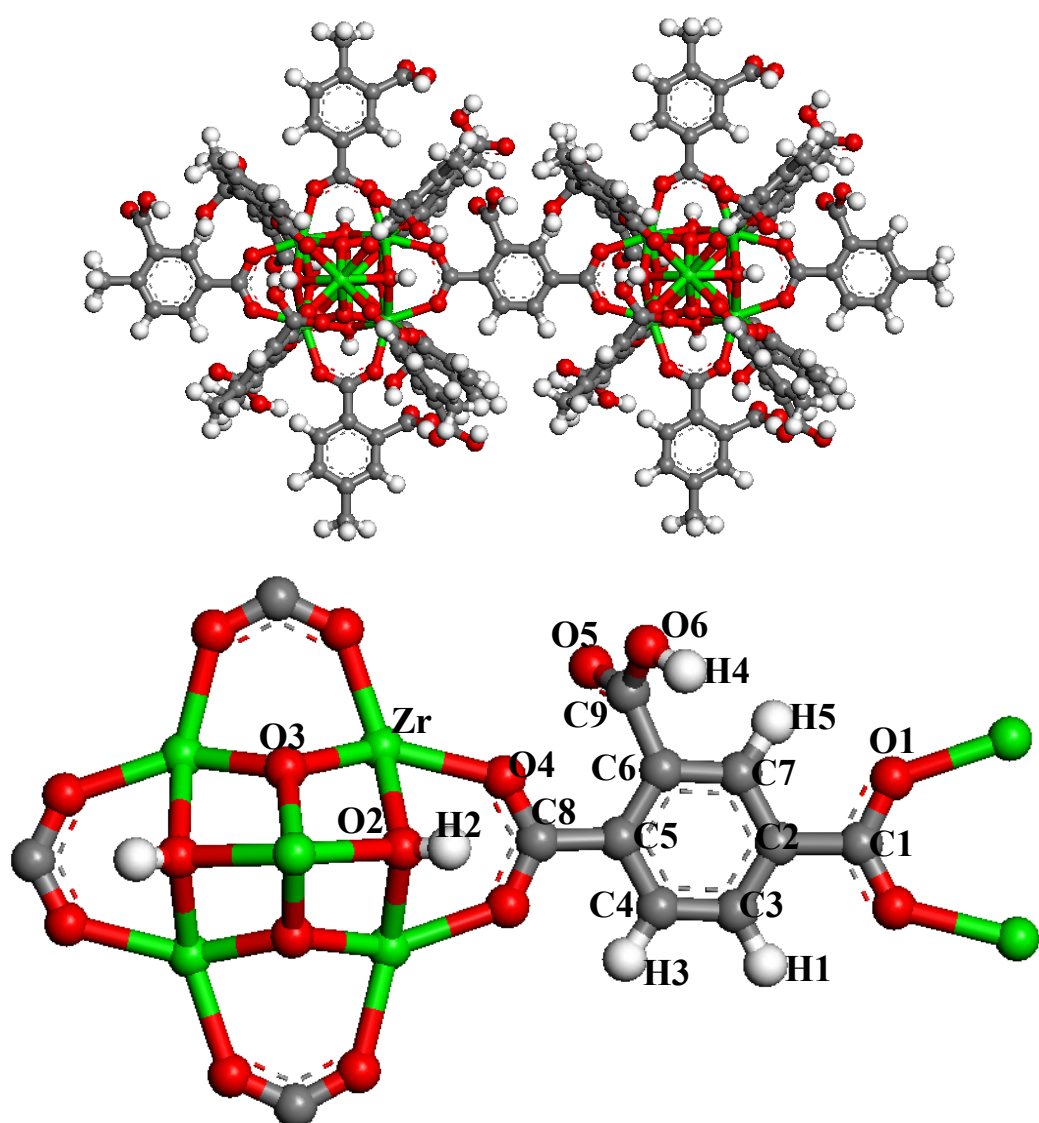


**Fig. S7.** Cluster used for calculating partial charges on UiO-66(Zr)-CO<sub>2</sub>H atoms. The terminations of the cluster were saturated with methyl groups to minimize the boundary effects.

**Table S7.** Atomic partial charges for the UiO-66(Zr)-SO<sub>3</sub>H structure derived on DFT/PBE Level.

Atomic types	Zr	O1	O2	O3	O4	O5	O6	C1	C2
Charge (e)	2.138	-0.612	-1.142	-0.853	-0.625	-0.509	-0.529	0.672	0.032
Atomic types	C3	C4	C5	C6	C7	C8	C9	H1	H2
Charge (e)	-0.128	-0.092	-0.060	-0.113	-0.121	0.693	0.669	0.139	0.486
Atomic types	H3	H4	H5						
Charge (e)	0.127	0.386	0.163						

### 3.7 Model cluster and atomic partial charges of UiO-66(Zr)-SO<sub>3</sub>H

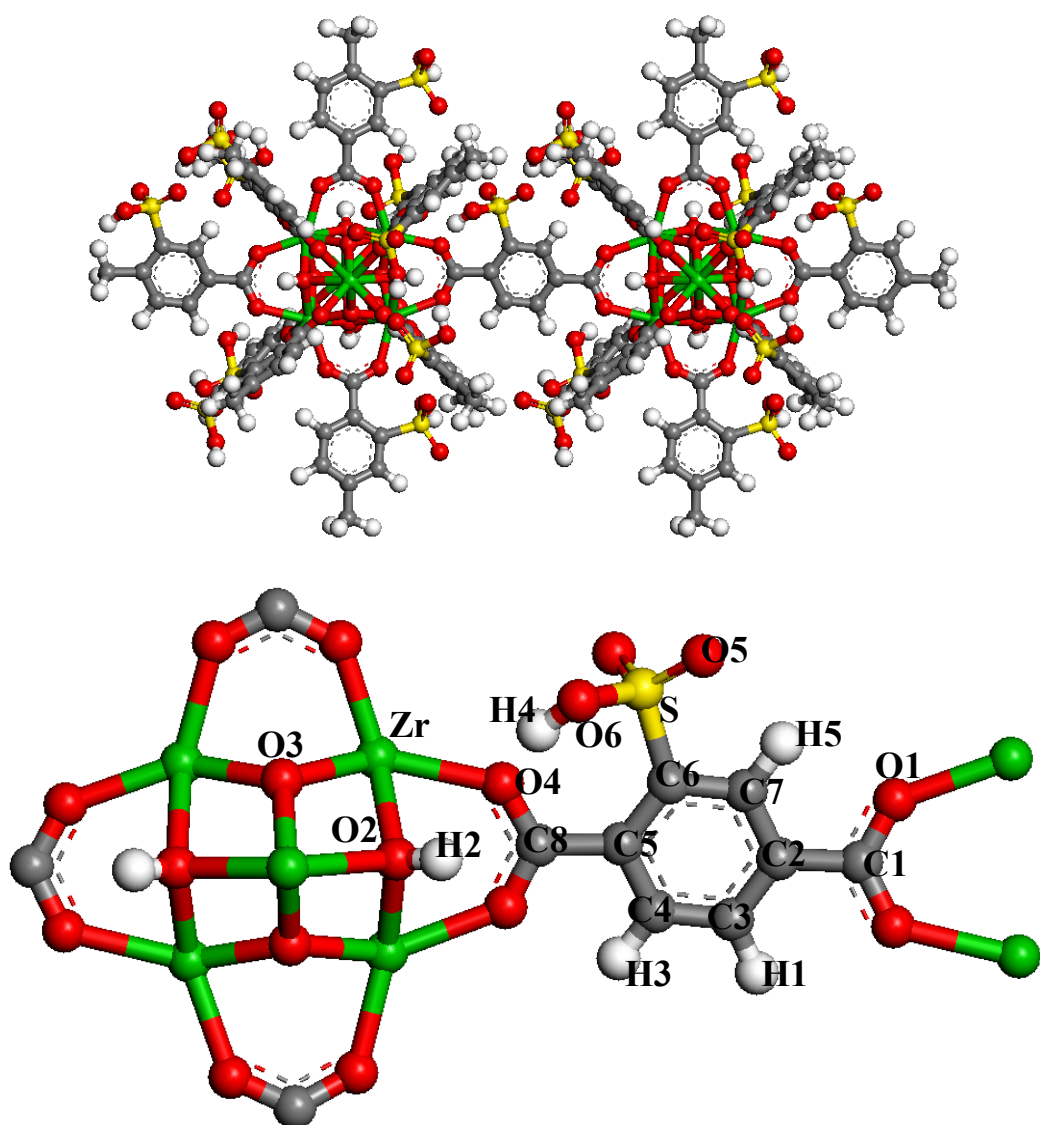


**Fig. S8.** Cluster used for calculating partial charges on UiO-66(Zr)-SO<sub>3</sub>H atoms. The terminations of the cluster were saturated with methyl groups to minimize the boundary effects.

**Table S8. Atomic partial charges for the UiO-66(Zr)-SO<sub>3</sub>H structure derived on DFT/PBE Level.**

Atomic types	Zr	O1	O2	O3	O4	O5	O6	C1	C2
Charge (e)	2.072	-0.572	-0.999	-0.881	-0.542	-0.492	-0.567	0.655	0.012
Atomic types	C3	C4	C5	C6	C7	C8	H1	H2	H3
Charge (e)	-0.141	-0.065	-0.076	-0.023	-0.129	0.599	0.140	0.431	0.126
Atomic types	H4	H5	S						
Charge (e)	0.419	0.147	1.039						

### 3.8 Model cluster and atomic partial charges of UiO-66(Zr)-(CF<sub>3</sub>)<sub>2</sub>

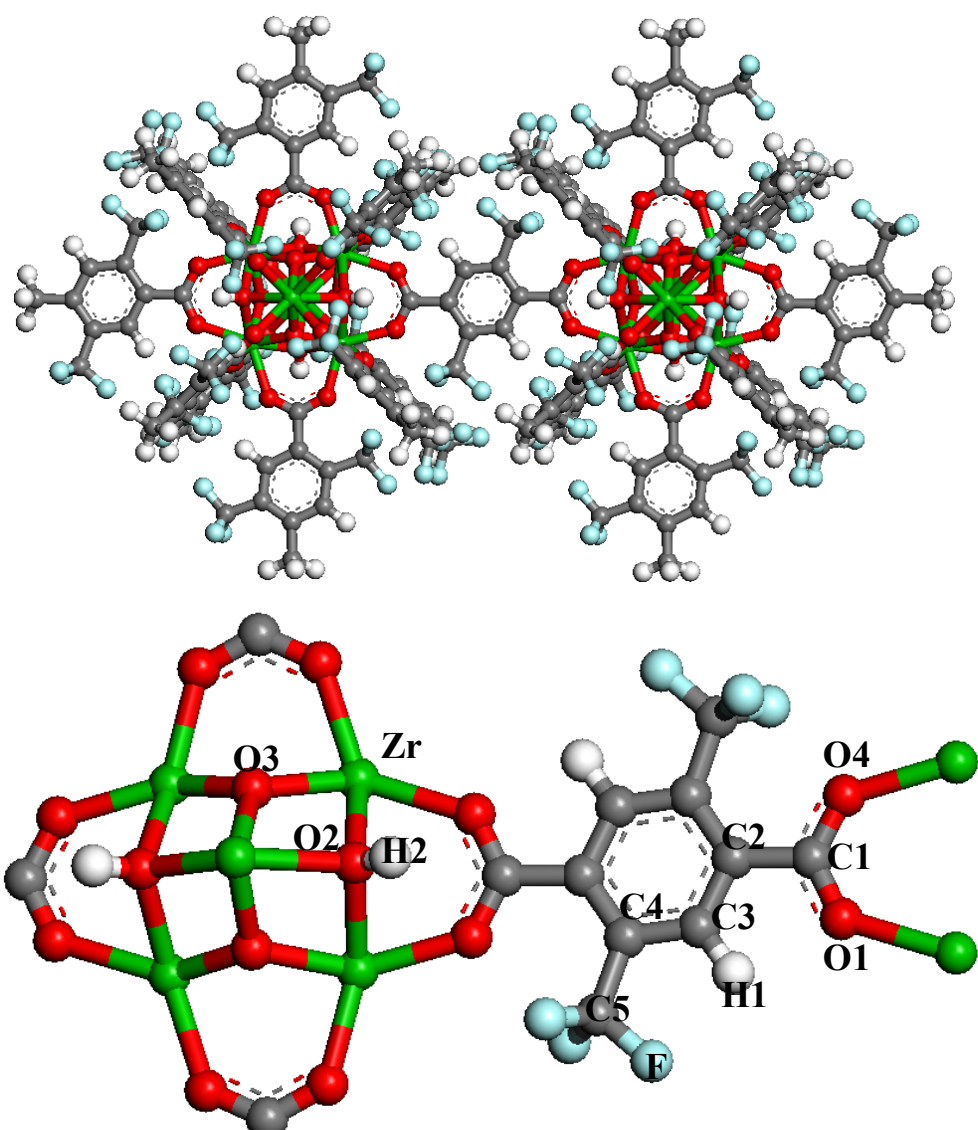


**Fig. S9.** Cluster used for calculating partial charges on UiO-66(Zr)-(CF<sub>3</sub>)<sub>2</sub> atoms. The terminations of the cluster were saturated with methyl groups to minimize the boundary effects.

**Table S9.** Atomic partial charges for the UiO-66(Zr)-(CF<sub>3</sub>)<sub>2</sub> structure derived on DFT/PBE Level.

Atomic types	Zr	O1	O2	O3	O4	C1	C2	C3
Charge (e)	2.100	-0.602	-0.102	-0.824	-0.568	0.665	-0.011	-0.118
Atomic types	C4	C5	H1	H2	F			
Charge (e)	-0.090	0.659	0.154	0.480	-0.219			

#### 4. Interatomic Potentials

Successful investigation of the adsorption/diffusion behavior of fluid in MOFs requires an accurate description of the interactions between adsorbate-adsorbate and adsorbate-MOF. In this present work, a single LJ interaction site model was used to describe a CH<sub>4</sub> molecule with potential parameters taken from the TraPPE forcefield.<sup>15a</sup> The CO<sub>2</sub> molecule was represented by the conventional rigid linear triatomic model with three charged LJ interaction sites (C–O bond length of 1.149 Å) located on each atom as previously described by Harris and Yung.<sup>15b</sup> All the corresponding atomic partial charges and interatomic potential parameters are reported in Table S10. The interactions between CO<sub>2</sub> and the surface of the UiO-66(Zr) series were described by a combination of site-site LJ and Coulombic potentials, while the interactions between CH<sub>4</sub> and UiO-66(Zr) series were only treated using a site-site LJ potential. The LJ potential parameters for the framework atoms of MOFs studied in these work were taken from DREIDING<sup>16</sup> and Universal (UFF)<sup>4</sup> force fields for CH<sub>4</sub> and CO<sub>2</sub> respectively, as given in Table S11. All the LJ cross interaction parameters including adsorbate/adsorbate and adsorbate/MOF were determined by the Lorentz-Berthelot mixing rule. The above set of force fields has been validated in our previous work for the dehydroxylated form of the non-modified UiO-66(Zr), where both the simulated isotherms and low-coverage adsorption enthalpies of CH<sub>4</sub> and CO<sub>2</sub> were in good agreement with the gravimetric and calorimetric measurements.<sup>1b</sup> Thus, to be consistent, the same force field were also adopted in current work. Actually, when one deals with the adsorption of CH<sub>4</sub> or alkanes in MOF materials, one can find in the literature that the description of the framework via the DREIDING forcefield usually leads to a better agreement with the experimental results.<sup>18</sup> Similar observations were also found that the simulations with UFF force field lead to a better agreement with the experimental data on the CO<sub>2</sub> adsorption in various MOFs.<sup>19</sup>

**Table S10.** Potential parameters and partial charges for the adsorbates

Atomic type	$\sigma$ (Å)	$\varepsilon$ /k <sub>B</sub> (K)	q (e)
CH <sub>4</sub>	3.730	148.000	0.0000
CO <sub>2</sub> _C	2.757	28.129	0.6512
CO <sub>2</sub> _O	3.033	80.507	-0.3256

**Table S11.** LJ potential parameters for the atoms of the UiO-66(Zr) series.

Elements	DREIDING		UFF	
	$\sigma$ (Å)	$\varepsilon$ /k <sub>B</sub> (K)	$\sigma$ (Å)	$\varepsilon$ /k <sub>B</sub> (K)
Zr	2.783 <sup>a</sup>	34.724 <sup>a</sup>	2.783	34.724
C	3.473	47.859	3.431	52.841
O	3.033	48.161	3.118	30.195
H	2.846	7.649	2.571	22.143
N	3.263	38.951	3.261	34.724
Br	3.519	186.202	3.732	126.315
F	3.093	36.485	2.997	25.162
S	3.590	173.117	3.595	137.890

<sup>a</sup> taken from UFF.

## 5. Details of the molecular Simulations

Grand canonical Monte Carlo (GCMC) simulations were performed to investigate the adsorption of the single components CO<sub>2</sub> and CH<sub>4</sub> and their binary equimolar mixtures (50/50) in the MOFs at 303 K, using our newly developed simulation code CADSS (Complex Adsorption and Diffusion Simulation Suite). For the simulations of pure components, molecules involve four types of trials: attempts (i) to displace a molecule (translation or rotation), (ii) to regrow a molecule at a random position, (iii) to create a new molecule, and (iv) to delete an existing molecule. For the simulations of mixture, attempt to exchange molecular identity was introduced as an additional type of trial to speed up the equilibrium and reduce the statistical errors. Details on the method can be found elsewhere.<sup>19</sup> The simulation box consisted of 27 (3×3×3) primitive cells for each modified UiO-66(Zr) form. A cutoff radius of 14.0 Å was applied to the Lennard-Jones (LJ) interactions, while the long-range electrostatic interactions were

handled by the Ewald summation technique. Periodic boundary conditions were considered in all three dimensions. Peng-Robinson equation of state was used to convert the pressure to the corresponding fugacity used in the GCMC simulations. As the adsorbents were maintained fixed during the simulations, the potential energies between an adsorbate and the adsorbent were initially tabulated on a series of three-dimensional grid points with grid spacing 0.15 Å. During the simulations, the potential energy at any position of the adsorbent was determined by interpolation. For each state point, GCMC simulations consisted of  $2 \times 10^7$  steps to ensure the equilibration, followed by  $2 \times 10^7$  steps to sample the desired thermodynamic properties. For the calculation of the adsorption enthalpies ( $\Delta H$ ) of CH<sub>4</sub> and CO<sub>2</sub> at the limit of zero coverage, configurational-bias Monte Carlo simulations in the canonical (NVT) ensemble were further performed using the revised Widom's test particle method.<sup>20</sup> In addition, the radial distribution functions (RDFs) between the guest molecules and both the  $\mu_3$ -OH and the grafting groups at three pressures (0.1, 1.0, 10. bar) were calculated for CH<sub>4</sub> and CO<sub>2</sub> in each adsorbent using the NVT Monte Carlo simulations. Each NVT MC run consisted of  $1 \times 10^7$  equilibration steps followed by another  $1 \times 10^7$  production steps where the RDFs were sampled at an interval of 1000 steps.

## 6. Comparison of the isotherms

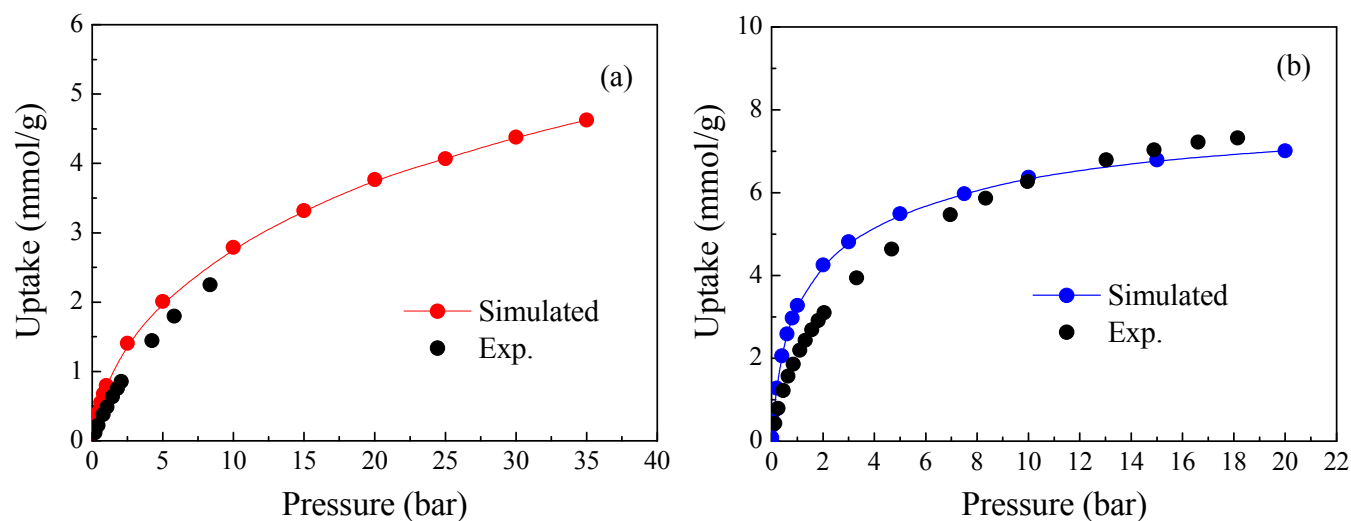


**Fig. S10.** Comparison of the simulated isotherms of the pure gases with the experimental data in the nonmodified UiO-66(Zr) at 303 K: (a)  $\text{CH}_4$ , (b)  $\text{CO}_2$ .

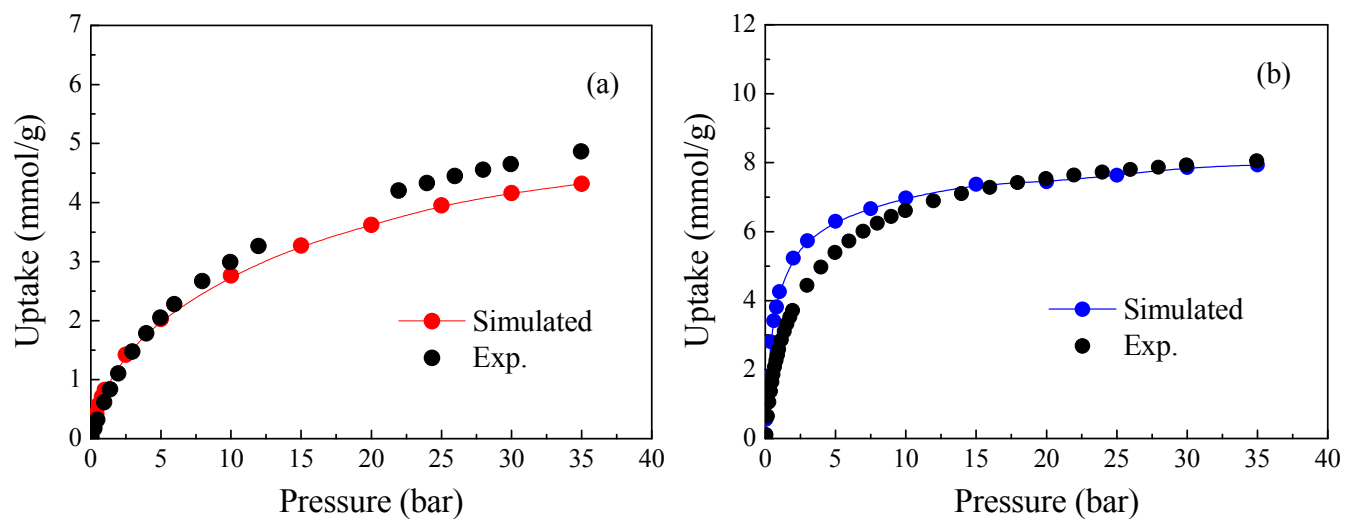


**Fig. S11.** Comparison of the simulated isotherms of the pure gases with the experimental data in the amino-functionalized material UiO-66(Zr)-NH<sub>2</sub> at 303 K: (a)  $\text{CH}_4$ , (b)  $\text{CO}_2$ .

## 7. Radial Distribution Functions calculated in the UiO-66(Zr) series

### 7.1 CO<sub>2</sub> and CH<sub>4</sub> gases in the non modified UiO-66(Zr)

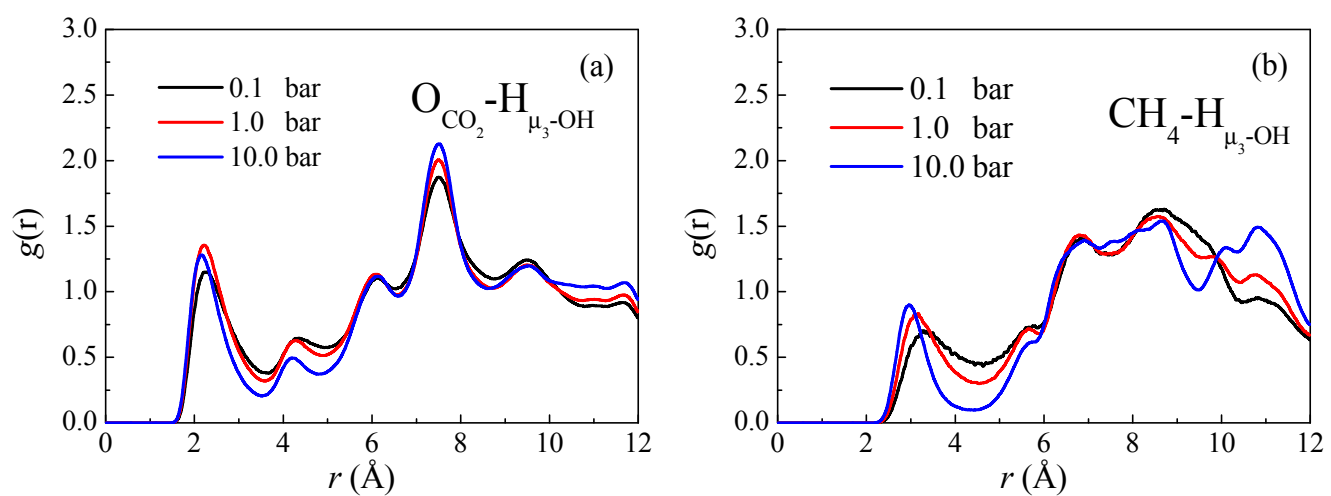


**Fig. S12.** Radial distribution functions of the adsorbate molecules around the H atoms of the  $\mu_3\text{-OH}$  groups in the non modified UiO-66(Zr) at three pressures: (a) CO<sub>2</sub>, (b) CH<sub>4</sub>.

## 7.2 CO<sub>2</sub> and CH<sub>4</sub> gases in the UiO-66(Zr)-CO<sub>2</sub>H

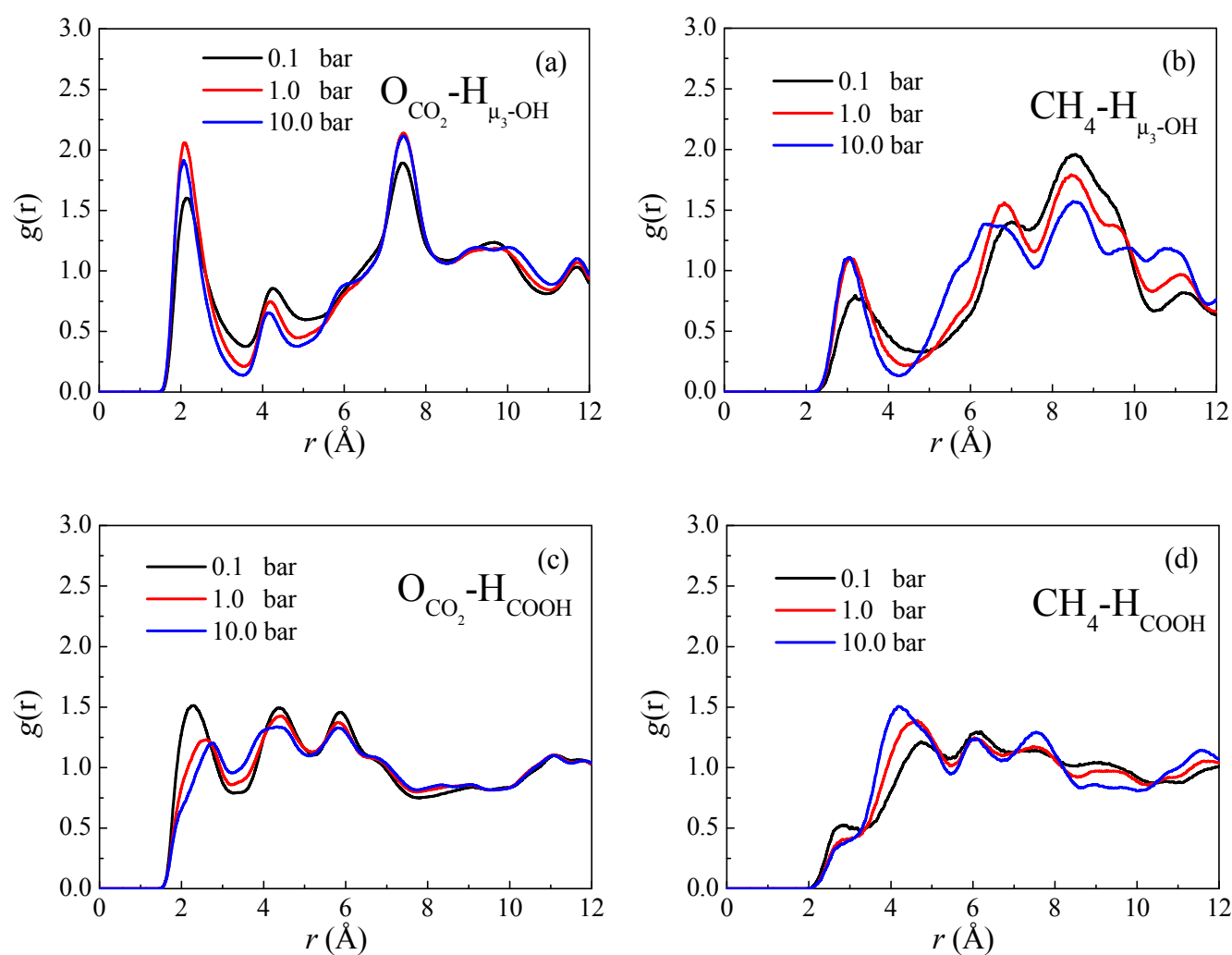


**Fig. S13.** Radial distribution functions of the adsorbate molecules around the H atoms of the  $\mu_3\text{-OH}$  groups (a, b) and of the carboxylate groups (c, d) in the functionalized material UiO-66(Zr)-CO<sub>2</sub>H at three pressures: (a, c) CO<sub>2</sub>, (b, d) CH<sub>4</sub>.

### 7.3 CO<sub>2</sub> and CH<sub>4</sub> gases in the UiO-66(Zr)-SO<sub>3</sub>H

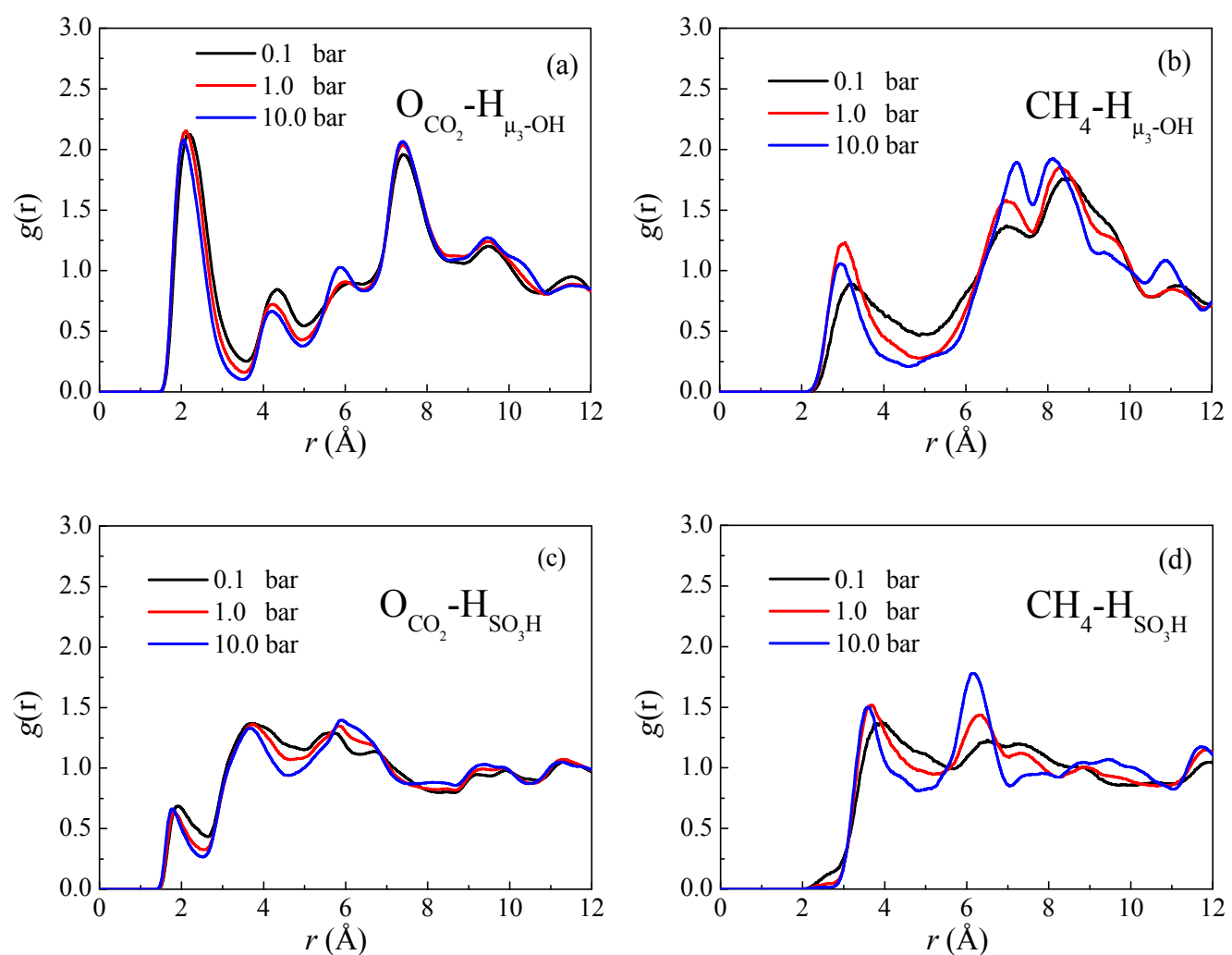


**Fig. S14.** Radial distribution functions of the adsorbate molecules around the H atoms of the  $\mu_3$ -OH groups (a, b), and of the sulfonic groups (c, d) in the functionalized material UiO-66(Zr)-SO<sub>3</sub>H at three pressures: (a, c) CO<sub>2</sub>, (b, d) CH<sub>4</sub>.

## 7.4 CO<sub>2</sub> and CH<sub>4</sub> gases in the UiO-66(Zr)-NH<sub>2</sub>

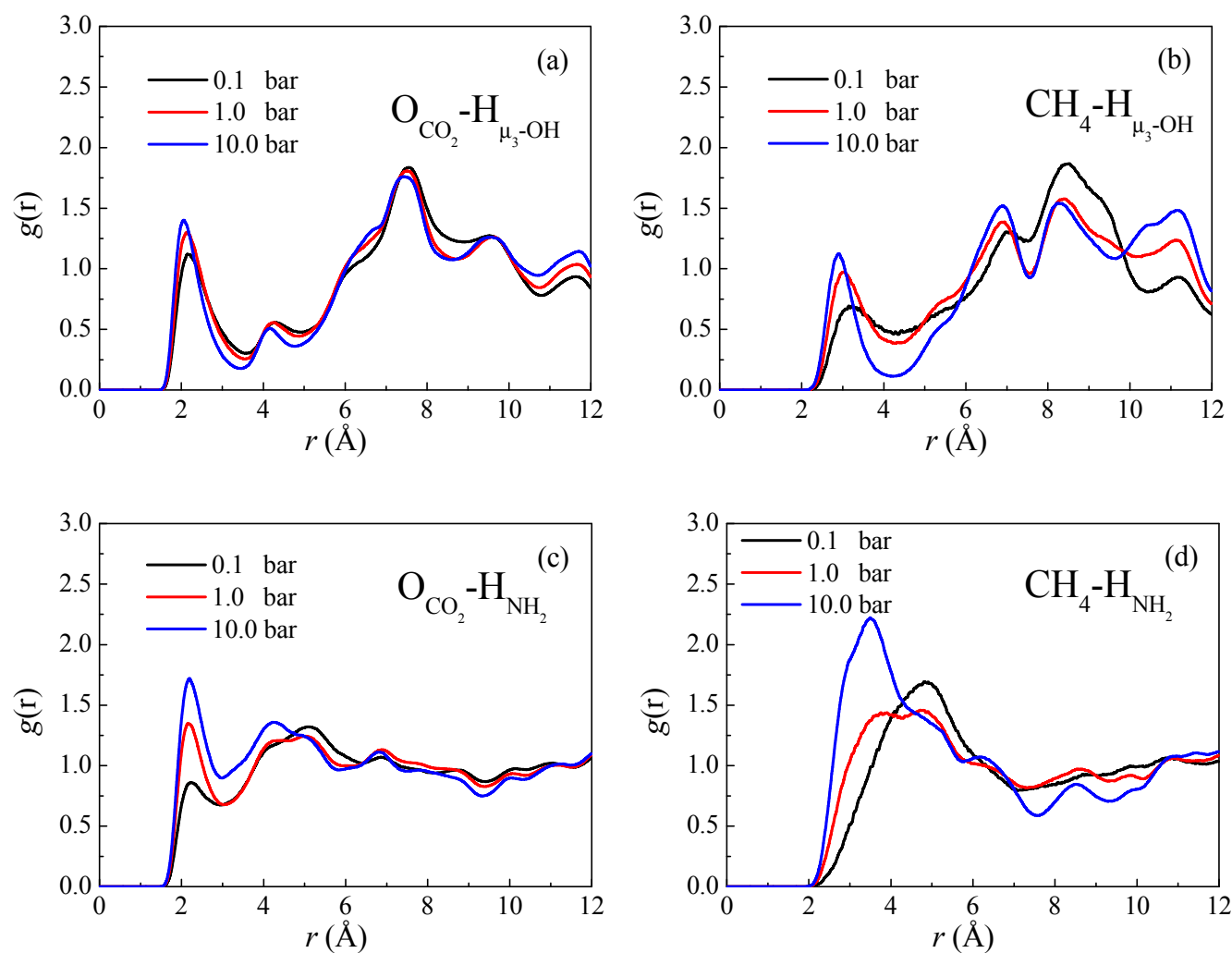


**Fig. S15.** Radial distribution functions of the adsorbate molecules around the H atoms of the  $\mu_3\text{-OH}$  groups (a, b) and of the amino groups (c, d) in the functionalized material UiO-66(Zr)-NH<sub>2</sub> at three pressures: (a, c) CO<sub>2</sub>, (b, d) CH<sub>4</sub>.

## 7.5 CO<sub>2</sub> and CH<sub>4</sub> gases in the UiO-66(Zr)-(OH)<sub>2</sub>

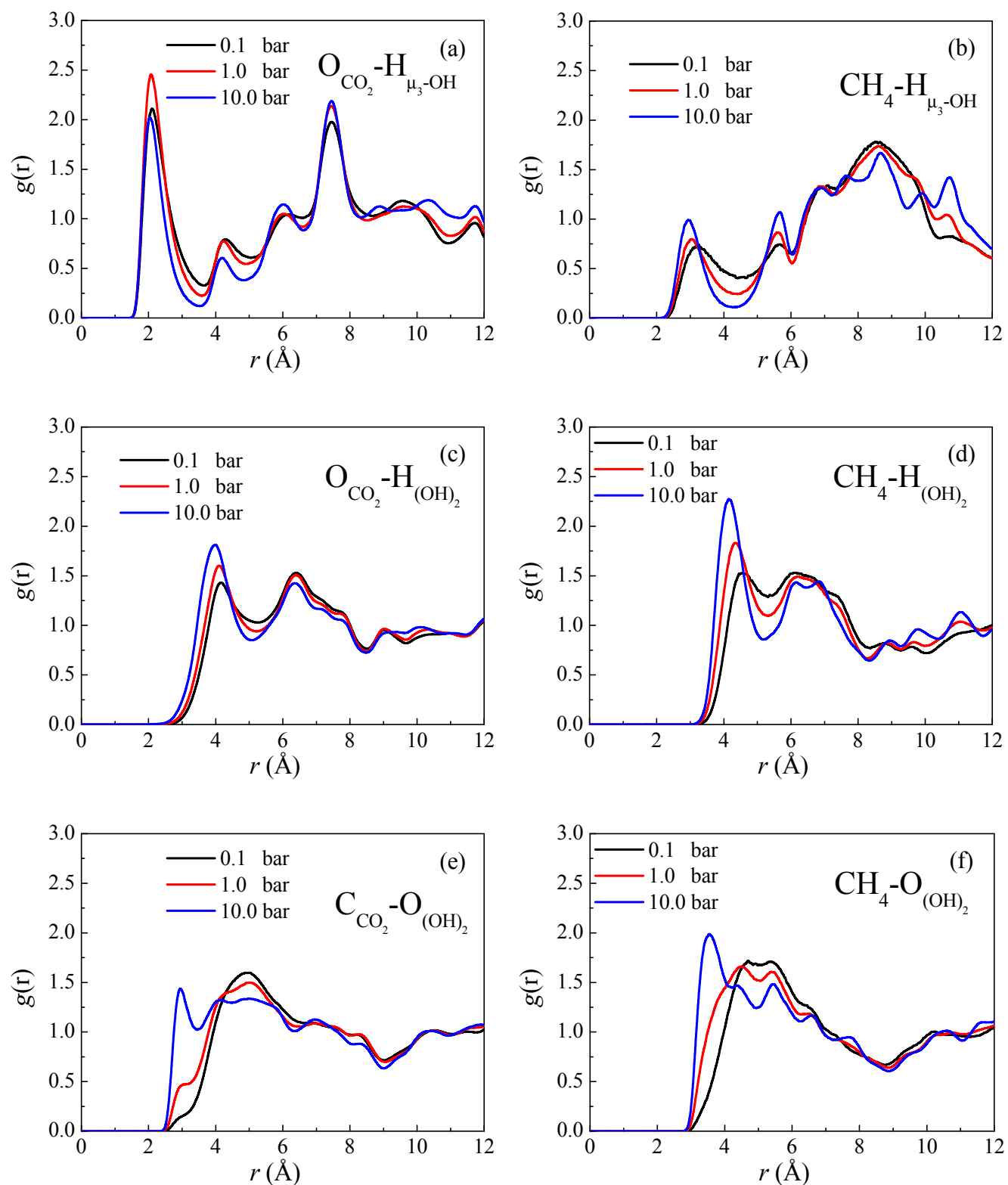


**Fig. S16.** Radial distribution functions of the adsorbate molecules around the H atoms of the  $\mu_3\text{-OH}$  groups (a, b) and of the hydroxyl groups (c, d) in the functionalized material UiO-66(Zr)-(OH)<sub>2</sub> at three pressures: (a, c, e) CO<sub>2</sub>, (b, d, f) CH<sub>4</sub>.

## 7.6 CO<sub>2</sub> and CH<sub>4</sub> gases in the UiO-66(Zr)-Br

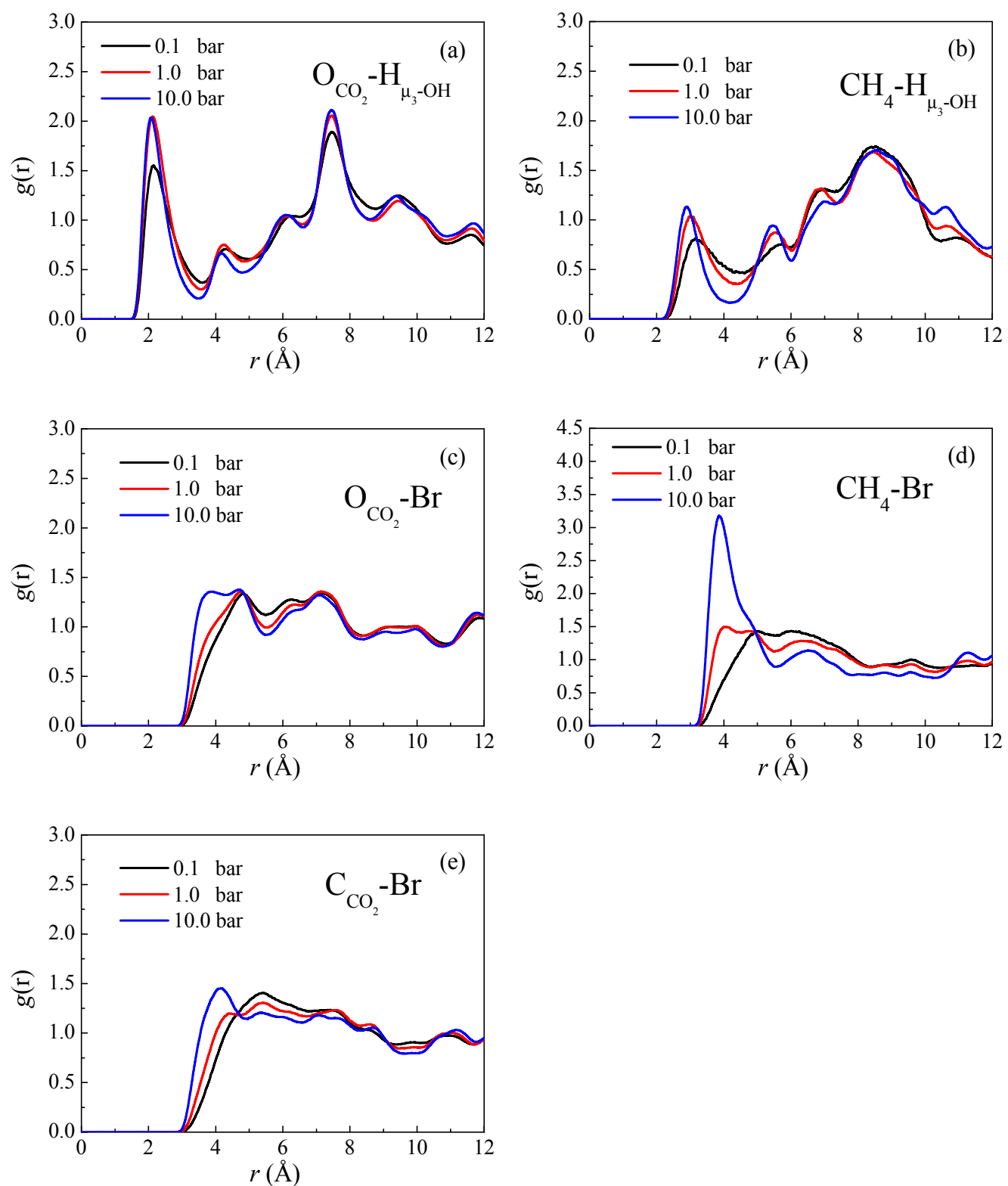


**Fig. S17.** Radial distribution functions of the adsorbate molecules around the H atoms of the  $\mu_3$ -OH groups (a, b) and the bromine atoms (c, d, e) in the functionalized material UiO-66(Zr)-Br at three pressures: (a, c, e) CO<sub>2</sub>, (b, d) CH<sub>4</sub>.

## 7.7 CO<sub>2</sub> and CH<sub>4</sub> gases in the UiO-66(Zr)-NO<sub>2</sub>

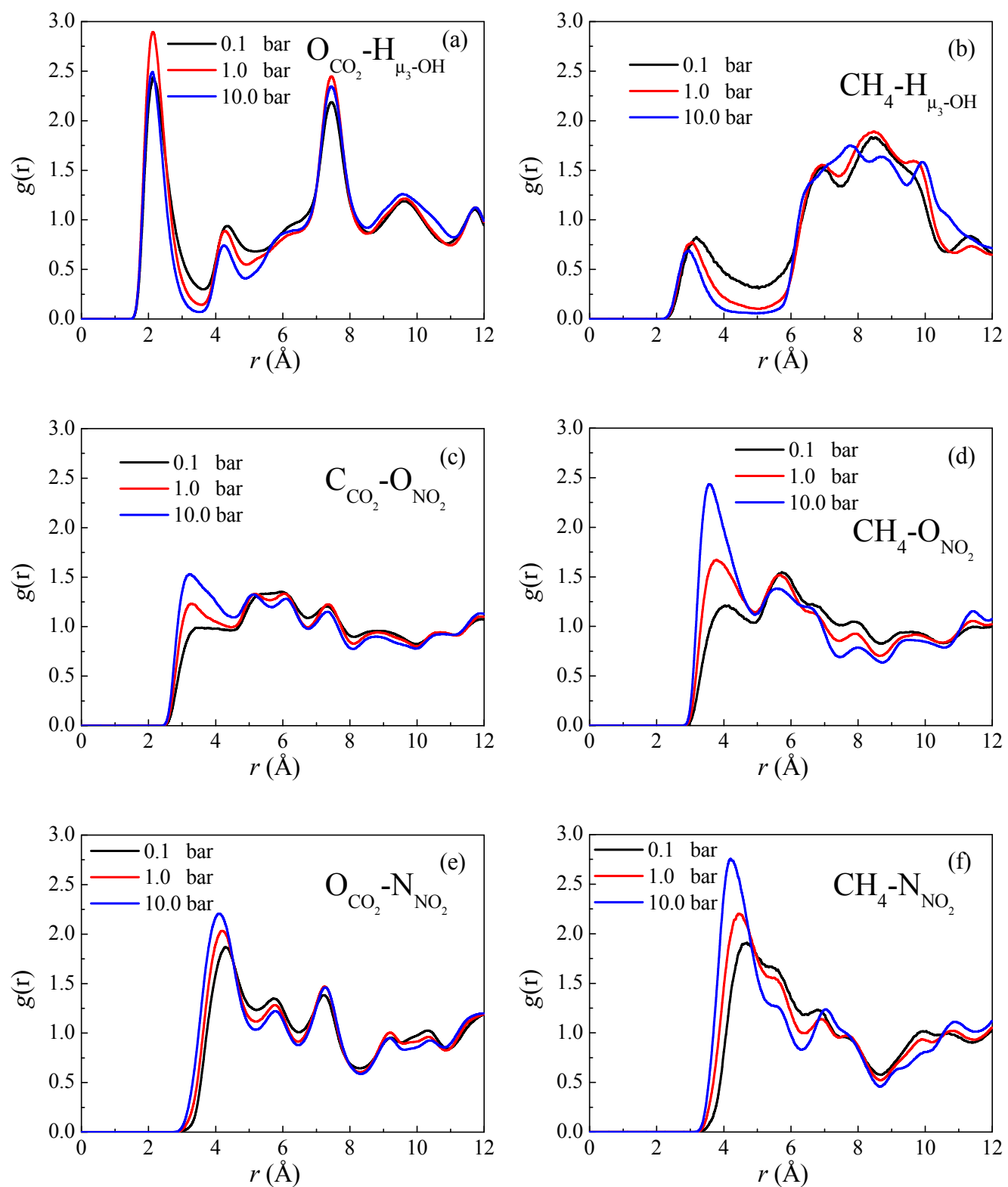


**Fig. S18.** Radial distribution functions of the adsorbate molecules around the H atoms of the  $\mu_3\text{-OH}$  groups (a, b) and the nitro groups (c, d, e, f) in the functionalized material UiO-66(Zr)-NO<sub>2</sub> at three pressures: (a, c, e) CO<sub>2</sub>, (b, d, f) CH<sub>4</sub>.

## 7.8 CO<sub>2</sub> and CH<sub>4</sub> gases in the UiO-66(Zr)-(CF<sub>3</sub>)<sub>2</sub>

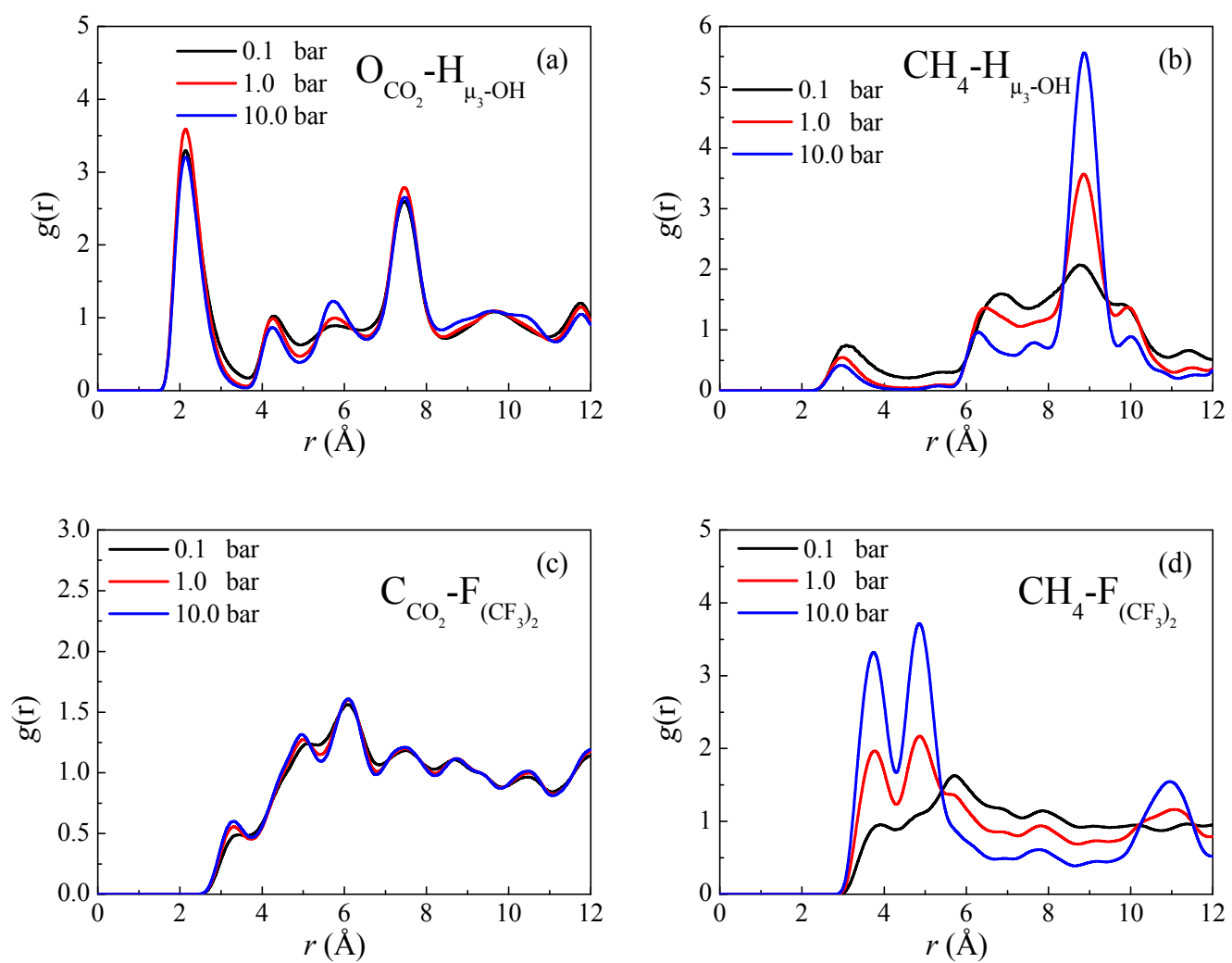


**Fig. S19.** Radial distribution functions of the adsorbate molecules around the H atoms of the  $\mu_3$ -OH groups (a, b) and the F atoms of the carbon trifluoride groups (c, d, e, f) in the functionalized material UiO-66(Zr)-(CF<sub>3</sub>)<sub>2</sub> at three pressures: (a, c) CO<sub>2</sub>, (b, d) CH<sub>4</sub>.

## 8. Effect of the functionalization on the separation of CO<sub>2</sub>/CH<sub>4</sub> mixture

In separation processes, a good indication of the separation ability consists of estimating the selectivity of a porous material. The selectivity (S) for CO<sub>2</sub> over CH<sub>4</sub> is defined by the following expression:  $S = (x_{CO_2} / x_{CH_4})(y_{CH_4} / x_{CO_2})$ , where  $x_{CO_2}$  and  $x_{CH_4}$  are the mole fractions of CO<sub>2</sub> and CH<sub>4</sub> in the adsorbed phase, respectively, while  $y_{CO_2}$  and  $y_{CH_4}$  are the mole fractions of CO<sub>2</sub> and CH<sub>4</sub> in the bulk phase, respectively. The calculated selectivities for their equimolar mixture in various functionalized UiO-66(Zr) are shown in Figure S11 as a function of the bulk pressure.

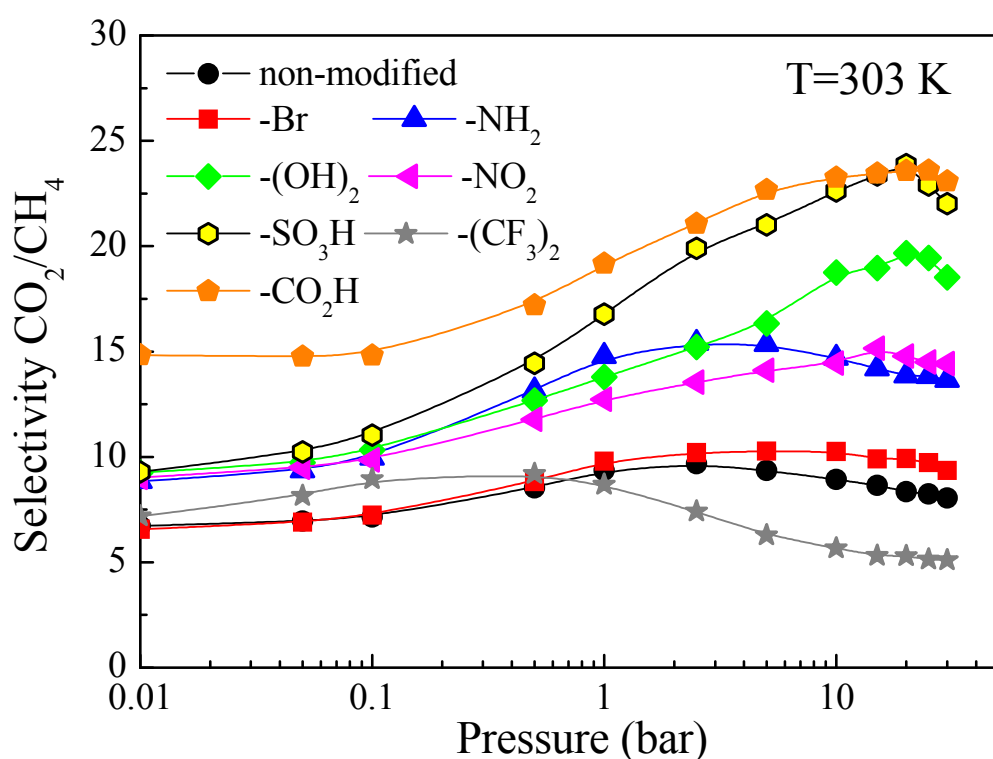


**Fig. S20.** Simulated selectivities for CO<sub>2</sub> over CH<sub>4</sub> from their equimolar gas mixture at 303 K in the non modified UiO-66(Zr) and its various functionalized forms, as a function of the bulk pressure.

## 9. Effect of the bulk composition on the separation of the CO<sub>2</sub>/CH<sub>4</sub> mixture

To study the effect of the bulk composition on the separation of the CO<sub>2</sub>/CH<sub>4</sub> mixture, GCMC simulations were further carried out for two other bulk compositions (CO<sub>2</sub> : CH<sub>4</sub> = 25 : 75 and 10 : 90). As a typical illustration, the simulated adsorption selectivities in the nonmodified UiO-66(Zr), UiO-66(Zr)-SO<sub>3</sub>H and UiO-66(Zr)-CO<sub>2</sub>H solids are shown in Figure S21 as a function of the total pressure up to 30 bar. The previous results for the equimolar mixture are also shown in this Figure as a comparison. As can be seen in this figure, the CO<sub>2</sub>/CH<sub>4</sub> selectivities in all three materials only weakly depend on the bulk composition within the pressure range considered in this work. Such bulk composition dependence of the adsorption selectivities was also found to be very similar in other materials examined in this study.

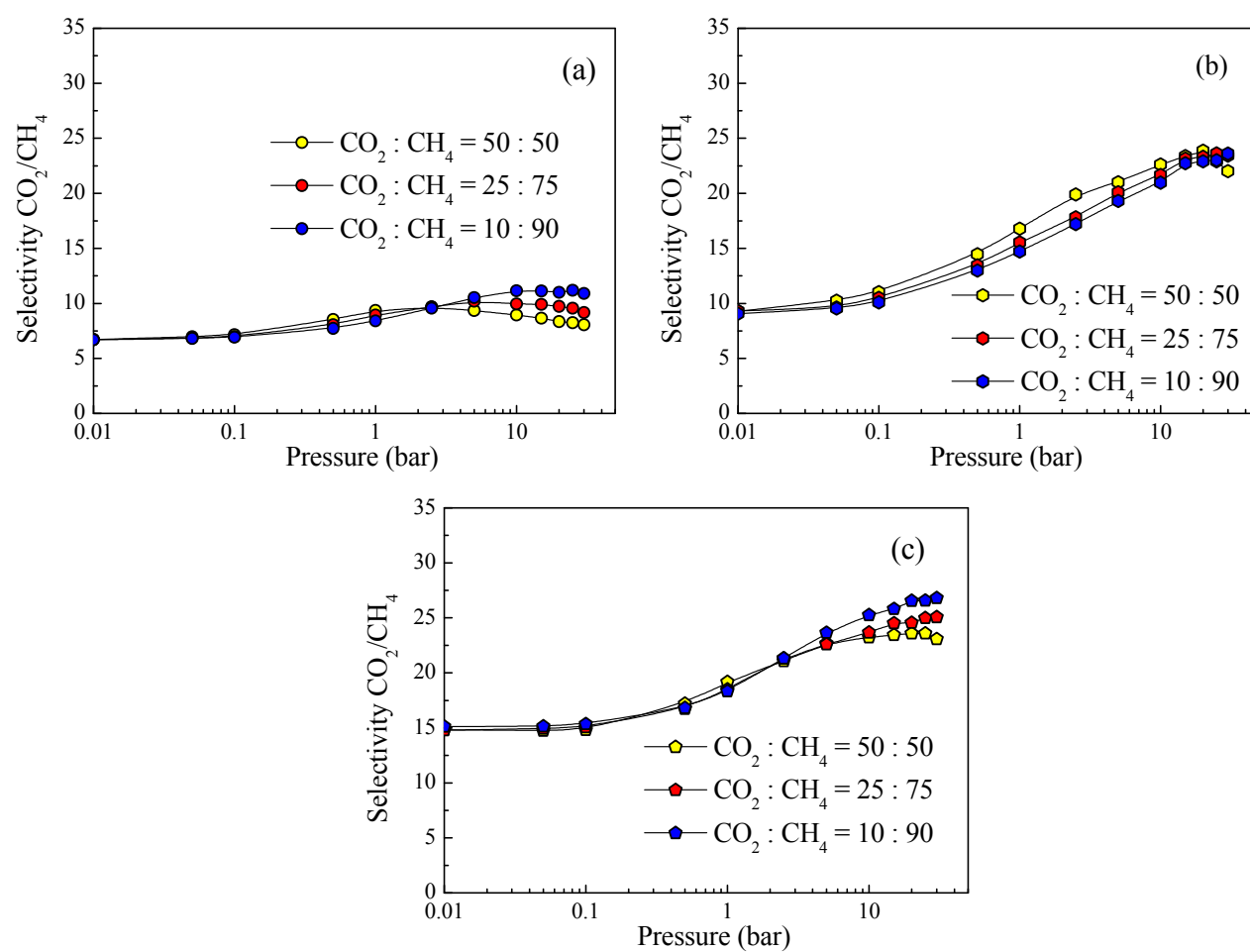


**Fig. S21.** Effect of the bulk composition on the adsorption selectivities for CO<sub>2</sub> over CH<sub>4</sub> from their gas mixture at 303 K, as a function of the bulk pressure: (a) nonmodified UiO-66(Zr), (b) UiO-66(Zr)-SO<sub>3</sub>H, (c) UiO-66(Zr)-CO<sub>2</sub>H.

## References:

- (1) C. Serre et al., in preparation
- (2) G. De Weireld, M. Frere and R. Jadot, *Meas. Sci. Technol.*, 1999, **10**, 117.
- (3) A. Ghoufi, L. Gaberova, L. Rouquerol, D. Vincent, P. L. Llewellyn and G. Maurin, *Microporous Mesoporous Mater.*, 2009, **119**, 117.
- (4) (a) A. K. Rappé, C. J. Casewit, K. S. Colwell, W. A. Goddard III and W. M. Skiff, *J. Am. Chem. Soc.*, 1992, **114**, 10024; (b)
- (5) A. L. Myers, P. A. Monson, *Langmuir*, 2002, **18**, 10261.
- (6) O. Talu, A. L. Myers, *AIChE J.*, 2001, **47**, 1160.
- (7) T. Düren, F. Millange, G. Férey, K. S. Walton and R. Q. Snurr, *J. Phys. Chem. C*, 2007, **111**, 15350.
- (8) (a) Y.-S. Bae, K.L. Mulfort, H. Frost, P. Ryan, S. Punnathanam, L.J. Broadbelt, J.T. Hupp, R.Q. Snurr, *Langmuir*, 2008, **24**, 8592; (b) Q. Yang and C. Zhong, *ChemPhysChem*, 2006, **7**, 1417; (c) A. Torrisi, R. G. Bell and C. Mellot-Draznieks, *Cryst. Growth Des.*, 2010, **10**, 2839.
- (9) (a) H. Heinz and U. W. Suter, *J. Phys. Chem. B*, 2004, **108**, 18341; (b) G. S. Maciel and E. Garcia, *Chem. Phys. Lett.*, 2005, **409**, 29.
- (10) (a) D. Foguet-Albiol, T. A. O'Brien, W. Wernsdorfer, B. Moulton, M. J. Zaworotko, K. A. Abbound and G. Christou, *Angew. Chem., Int. Ed.*, 2005, **44**, 897; (b) E. R. Davidson and A. E. Clark, *J. Phys. Chem. A*, 2002, **106**, 7456.
- (11) M. J. Frisch, G. W. Trucks, H. B. Schlegel, G. E. Scuseria, M. A. Robb, J. R. Cheeseman, J. A. Montgomery, Jr., T. Vreven, K. N. Kudin, J. C. Burant, J. M. Millam, S. S. Iyengar, J. Tomasi, V. Barone, B. Mennucci, M. Cossi, G. Scalmani, N. Rega, G. A. Petersson, H. Nakatsuji, M. Hada, M. Ehara, K. Toyota, R. Fukuda, J. Hasegawa, M. Ishida, T. Nakajima, Y. Honda, O. Kitao, H. Nakai, M. Klene, X. Li, J. E. Knox, H. P. Hratchian, J. B. Cross, V. Bakken, C. Adamo, J. Jaramillo, R. Gomperts, R. E. Stratmann, O. Yazyev, A. J. Austin, R. Cammi, C. Pomelli, J. W. Ochterski, P. Y. Ayala, K. Morokuma, G. A. Voth, P. Salvador, J. J. Dannenberg, V. G. Zakrzewski, S. Dapprich, A. D. Daniels, M. C. Strain, O. Farkas, D. K. Malick, A. D. Rabuck, K. Raghavachari, J. B. Foresman, J. V. Ortiz, Q. Cui, A. G. Baboul, S. Clifford, J. Cioslowski, B. B. Stefanov, G. Liu, A. Liashenko, P. Piskorz, I. Komaromi, R. L. Martin, D. J. Fox, T. Keith, M. A. Al-Laham, C. Y. Peng, A. Nanayakkara, M. Challacombe, P. M. W. Gill, B. Johnson, W. Chen, M. W. Wong, C. Gonzalez, and J. A. Pople, *GAUSSIAN 03*, Revision E.01, Gaussian, Inc., Wallingford CT, 2004.
- (12) A. Bondi, *J. Phys. Chem.* 1964, **68**, 441
- (13) B. Cordero, V. Gomez, A. E. Platero-Prats, M. Reves, J. Echeverria, E. Cremades, F. Barragan and S. Alvarez, *Dalton Trans.* 2008, **21**, 2832.
- (14) E. Haldoupis, S. Nair and D. S. Sholl, *J. Am. Chem. Soc.*, 2010, **132**, 7528.

- (15) (a) M. G. Martin and J. I. Siepmann, *J. Phys. Chem. B*, 1998, **102**, 2569; (b) J. G. Harris and K. Hung, *J. Phys. Chem.*, 1995, **99**, 12021.
- (16) S. L. Mayo, B. D. Olafson, W. A. Goddard III, *J. Phys. Chem.*, 1990, **94**, 8897.
- (17) (a) T. Duren and R. Q. Snurr, *J. Phys. Chem. B* **2004**, *108*, 15703; (b) Finsy, V.; Calero, S.; García-Pérez, E.; Merkling, P. J.; Vedts, G.; De Vos, D. E.; Baron, G. V. ; Denayer, L. F. M. *Phys. Chem. Chem. Phys.* **2009**, *11*, 3515.
- (18) (a) W. Morris, B. Leung, H. Furukawa, O. K. Yaghi, N. He, H. Hayashi, Y. Houndoungbo, M. Asta, B. B. Laird and O. M. Yaghi, *J. Am. Chem. Soc.*, 2010, **132**, 11006; (b) A. Sirjoosinhg, S. Alavi and T. K. Woo, *J. Phys. Chem. C*, 2010, **114**, 2171; (c) R. Babarao and J. W. Jiang, *Langmuir*, 2008, **24**, 6270.
- (19) Q. Yang and C. Zhong, *J. Phys. Chem. B*, 2006, **110**, 17776.
- (20) T. J. H. Vlugt, E. García-Pérez, D. Dubbeldam, S. Ban and S. Calero, *J. Chem. Theory Comput.*, 2008, **4**, 1107.